Eur. Phys. J. C 46, 413–420 (2006)
Digital Object Identifier (DOI) 10.1140/epjc/s2006-02517-7

THE EUROPEAN PHYSICAL JOURNAL C

Saturation in diffractive deep inelastic eA scattering

M.S. Kugeratski[1,a], V.P. Gonçalves[2,b], F.S. Navarra[1,c]

[1] Instituto de Física, Universidade de São Paulo, C.P. 66318, 05315-970 São Paulo, SP, Brazil
[2] High and Medium Energy Group (GAME), Instituto de Física e Matemática, Universidade Federal de Pelotas, Caixa Postal 354, CEP 96010-900, Pelotas, RS, Brazil

Received: 18 November 2005 / Revised version: 30 January 2006 /
Published online: 24 March 2006 –

Abstract. In this paper, we investigate the saturation physics in diffractive deep inelastic electron-ion scattering. We estimate the energy and nuclear dependence of the ratio $\sigma^{\rm diff}/\sigma^{\rm tot}$ and predict the $x_{I\!P}$ and β behavior of the nuclear diffractive structure function $F_{2,A}^{\rm D(3)}(Q^2,\beta,x_{I\!P})$. Moreover, we analyze the ratio $R_{A1,A2}^{\rm diff}(Q^2,\beta,x_{I\!P}) = F_{2,A1}^{D(3)}/F_{2,A2}^{D(3)}$, which probes the nuclear dependence of the structure of the pomeron. We show that saturation physics predicts that approximately 37% of the events observed at eRHIC should be diffractive.

1 Introduction

One of the frontiers of QCD intensely being investigated in high energy experiments is the high energy (small x) regime, where we expect to observe the non-linear behavior of the theory. In this regime, the growth of the parton distribution should saturate, forming a color glass condensate (CGC). (For recent reviews see, e.g. [1–4]). In fact, signals of parton saturation have already been observed both in ep deep inelastic scattering at HERA and in deuteron-gold collisions at RHIC (see, e.g. [5]). However, the observation of this new regime still needs confirmation and so there is an active search for new experimental signatures. Among them, the observables measured in diffractive deep inelastic scattering (DDIS) deserve special attention. As shown in [6], the total diffractive cross section is much more sensitive to large-size dipoles than the inclusive one. Saturation effects screen large-size dipole (soft) contributions, so that a fairly large fraction of the cross section is hard and hence eligible for a perturbative treatment. Therefore, the study of diffractive processes becomes fundamental in order to constrain the QCD dynamics at high energies.

Significant progress in understanding diffraction has been made with the ep collider HERA (see, e.g. [7–9]). Currently, there exist many attempts to describe the diffractive part of the deep inelastic cross section within pQCD (see, e.g. [6, 10–12]). One of the most successful approaches is the saturation approach [6] based on the dipole picture of DIS [13, 14]. It naturally incorporates the description of both inclusive and diffractive events in a common theoretical framework, as the same dipole scattering amplitude enters in the formulation of the inclusive and diffractive cross sections. In the studies of saturation effects in DDIS, non-linear evolution equations for the dipole scattering amplitude have been derived [15–18], new measurements proposed [19–22] and the charm contribution estimated [23]. However, as shown in [10], current data are not yet precise enough, nor do they extend to sufficiently small values of $x_{I\!P}$, to discriminate between different theoretical approaches.

Other sources of information on QCD dynamics at high parton density are due to nuclei that provide high density at comparatively lower energies. Recently, in [24], we estimated a set of inclusive observables that may be analyzed in a future electron-ion collider [25]. Our results have demonstrated that the saturation physics cannot be disregarded in the kinematical range of eRHIC. Our goal in this work is to understand to what extend the saturation regime of QCD manifests itself in diffractive deep inelastic eA scattering. In particular, we will study the energy and nuclear dependence of the ratio between diffractive and total cross sections ($\sigma_{\rm diff}/\sigma_{\rm tot}$). HERA has observed that the energy dependence of this ratio is almost constant for different mass intervals of the diffractively produced hadrons over a wide range of photon virtualities Q^2 [26]. This ratio is to a good approximation constant as a function of the Bjorken x variable and Q^2. Moreover, we make predictions for more detailed diffractive properties, such as those embodied in the diffractive structure function $F_2^{\rm D(3)}(Q^2,\beta,x_{I\!P})$. Motivated by [25, 27], we also analyze the behavior of the ratio between nuclear diffractive structure functions $R_{A1,A2}^{\rm diff}(Q^2,\beta,x_{I\!P} = F_{2,A1}^{\rm D(3)}/F_{2,A2}^{\rm D(3)}$, where A_1 and A_2 denote the atomic number of the two nuclei. It is important to emphasize that diffractive processes

[a] e-mail: msks@if.usp.br
[b] e-mail: barros@ufpel.edu.br
[c] e-mail: navarra@if.usp.br

in eA collisions were studied in [21, 28–35]. Here we extend these studies to a large number of observables, considering the dipole approach and a generalization for nuclear targets of the CGC dipole cross section proposed in [36]. As this model successfully describes the HERA data, we believe that it is possible to obtain realistic predictions for the kinematical range of the electron-ion collider eRHIC.

This paper is organized as follows. In next section, we present a brief review of the dipole picture. We present the main formulae for the dipole cross section and the diffractive structure function. In Sect. 3 we introduce the overlap function for diffractive events, which allows us to find the average dipole size that contributes the most to this process, and analyze its dipole size and nuclear dependences. Moreover, we estimate the different contributions to the diffractive structure function and present our predictions for $F_2^{\mathrm{D}(3)}$ and $R_{A1,A2}^{\mathrm{diff}}$. Finally, in Sect. 4 we summarize our main conclusions.

2 Dipole picture of diffractive DIS

In deep inelastic scattering, a photon of virtuality Q^2 collides with a target. In an appropriate frame, called the dipole frame, the virtual photon undergoes hadronic interaction via a fluctuation into a dipole. The wave functions $|\psi_{\mathrm{T}}|^2$ and $|\psi_{\mathrm{L}}|^2$, describing the splitting of the photon on the dipole, are given by [13]:

$$|\psi_{\mathrm{L}}(\alpha,r)|^2 = \frac{3\alpha_{\mathrm{em}}}{\pi^2}\sum_f e_f^2 4Q^2\alpha^2(1-\alpha)^2K_0^2(\epsilon r)\,, \quad (1)$$

$$|\psi_{\mathrm{T}}(\alpha,r)|^2 = \frac{3\alpha_{\mathrm{em}}}{2\pi^2}\sum_f e_f^2\left\{[\alpha^2+(1-\alpha)^2]\epsilon^2K_1^2(\epsilon r) + m_f^2K_0^2(\epsilon r)\right\} \quad (2)$$

for a longitudinally and transversely polarized photon, respectively. In the above expressions $\epsilon^2=\alpha(1-\alpha)Q^2+m_f^2$, K_0 and K_1 are modified Bessel functions and the sum is over quarks of flavor f with a corresponding quark mass m_f. As usual, α stands for the longitudinal photon momentum fraction carried by the quark and $1-\alpha$ is the longitudinal photon momentum fraction of the antiquark. The dipole then interacts with the target and one has the following factorized formula [13]

$$\sigma_{\mathrm{L,T}}^{\gamma^*A}(x,Q^2) = \int \mathrm{d}\alpha\,\mathrm{d}^2\boldsymbol{r}\,|\psi_{\mathrm{L,T}}(\alpha,\boldsymbol{r})|^2\sigma_{\mathrm{dip}}(x,\boldsymbol{r})\,. \quad (3)$$

Similarly, the total diffractive cross sections take on the following form (see e.g. [6, 9, 13])

$$\sigma_{\mathrm{T,L}}^{\mathrm{D}} = \int_{-\infty}^{0}\mathrm{d}t\,e^{B_{\mathrm{D}}t}\left.\frac{\mathrm{d}\sigma_{\mathrm{T,L}}^{\mathrm{D}}}{\mathrm{d}t}\right|_{t=0} = \frac{1}{B_{\mathrm{D}}}\left.\frac{\mathrm{d}\sigma_{\mathrm{T,L}}^{\mathrm{D}}}{\mathrm{d}t}\right|_{t=0}, \quad (4)$$

where

$$\left.\frac{\mathrm{d}\sigma_{\mathrm{T,L}}^{\mathrm{D}}}{\mathrm{d}t}\right|_{t=0} = \frac{1}{16\pi}\int\mathrm{d}^2\mathbf{r}\int_0^1 d\alpha|\Psi_{T,L}(\alpha,\mathbf{r})|^2\sigma_{\mathrm{dip}}^2(x,r^2)\,, \quad (5)$$

and we have assumed a factorizable dependence on t with the diffractive slope B_{D}.

The diffractive process can be analyzed in more detail by studying the behavior of the diffractive structure function $F_2^{\mathrm{D}(3)}(Q^2,\beta,x_{I\!P}$. In [6, 13], the authors derived expressions for $F_2^{\mathrm{D}(3)}$ directly in the transverse momentum space and then transformed them to impact parameter space where the dipole approach can be applied. Following [6], we assume that the diffractive structure function is given by

$$F_2^{\mathrm{D}(3)}(Q^2,\beta,x_{I\!P} = F_{q\bar{q},\mathrm{L}}^{\mathrm{D}} + F_{q\bar{q},\mathrm{T}}^{\mathrm{D}} + F_{q\bar{q}g,\mathrm{T}}^{\mathrm{D}}\,, \quad (6)$$

where T and L refer to the polarization of the virtual photon. For the $q\bar{q}g$ contribution only the transverse polarization is considered, since the longitudinal counterpart has no leading logarithm in Q^2. The computation of the various contributions was made in [6, 13, 37] and here we quote only the final results:

$$x_{I\!P}F_{q\bar{q},\mathrm{L}}^{\mathrm{D}}(Q^2,\beta,x_{I\!P}) = \frac{3Q^6}{32\pi^4\beta B_{\mathrm{D}}}\sum_f e_f^2 2 \times\int_{\alpha_0}^{1/2}\mathrm{d}\alpha\alpha^3(1-\alpha)^3\Phi_0, \quad (7)$$

$$x_{I\!P}F_{q\bar{q},\mathrm{T}}^{\mathrm{D}}(Q^2,\beta,x_{I\!P}) = \frac{3Q^4}{128\pi^4\beta B_{\mathrm{D}}}\sum_f e_f^2 2\int_{\alpha_0}^{1/2}\mathrm{d}\alpha\alpha(1-\alpha) \times\left\{\epsilon^2[\alpha^2+(1-\alpha)^2]\Phi_1+m_f^2\Phi_0\right\}\,, \quad (8)$$

where the lower limit of the integral over α is given by $\alpha_0=\frac{1}{2}\left(1-\sqrt{1-\frac{4m_f^2}{M_X^2}}\right)$ and we have introduced the auxiliary functions [10]:

$$\Phi_{0,1}\equiv\left(\int_0^\infty r\mathrm{d}rK_{0,1}(\epsilon r)\sigma_{\mathrm{dip}}(x_{I\!P},rJ_{0,1}(kr)\right)^2. \quad (9)$$

For the $q\bar{q}g$ contribution, we have [6, 37, 38]

$$x_{I\!P}F_{q\bar{q}g,\mathrm{T}}^{\mathrm{D}}(Q^2,\beta,x_{I\!P}) = \frac{81\beta\alpha_{\mathrm{S}}}{512\pi^5B_{\mathrm{D}}}\sum_f e_f^2\int_\beta^1\frac{\mathrm{d}z}{(1-z)^3}\left[\left(1-\frac{\beta}{z}\right)^2+\left(\frac{\beta}{z}\right)^2\right] \times\int_0^{(1-z)Q^2}\mathrm{d}k_t^2\ln\left(\frac{(1-z)Q^2}{k_t^2}\right) \times\left[\int_0^\infty udu\,\sigma_{\mathrm{dip}}(u/k_t,x_{I\!P})K_2\left(\sqrt{\frac{z}{1-z}}u^2\right)J_2(u)\right]^2. \quad (10)$$

where β is an analogue of the Bjorken variable x for the diffractive system. We use the standard notation for variables $\beta=Q^2/(M_X^2+Q^2)$, $x_{I\!P}=(M_X^2+Q^2)/(W^2+Q^2)$ and $x=Q^2/(W^2+Q^2)=\beta x_{I\!P}$, where M_X is the invariant mass of the diffractive system and W the total energy of the γ^*p (or γ^*A). When extending (7), (8) and (10) to the

nuclear case, we need to change the slope to the nuclear slope parameter, B_A. In the following, we will assume that B_A may be approximated by $B_A = \frac{R_A^2}{4}$, where R_A is given by $R_A = 1.2A^{1/3}$ fm [39].

In the dipole picture, the behavior of the total inclusive and diffractive cross sections, as well as of the diffractive structure functions, is strongly dependent on the dipole cross section, which is determined by the QCD dynamics. Consequently, in the dipole picture, the inclusion of saturation physics is quite transparent and straightforward, as the dipole cross section is closely related to the solution of the QCD non-linear evolution equations (for recent reviews see, e.g. [1–4])

$$\sigma_{\rm dip}(x, \boldsymbol{r}) = 2 \int d^2\boldsymbol{b} \mathcal{N}(x, \boldsymbol{r}, \boldsymbol{b}) \ , \tag{11}$$

where $\mathcal{N}$ is the quark dipole-target forward scattering amplitude for a given impact parameter $\boldsymbol{b}$ that encodes all the information about the hadronic scattering, and thus about the non-linear and quantum effects in the hadron wave function. In the following, we will disregard the impact parameter dependence [$\sigma_{\rm dip} = \sigma_0 \mathcal{N}(x, \boldsymbol{r})$] and consider the phenomenological model proposed in [36], in which a parameterization of $\mathcal{N}(x, \boldsymbol{r})$ was constructed so as to reproduce two limits analytically under control: the solution of the BFKL equation for small dipole sizes, $\boldsymbol{r} \ll 1/Q_s(x)$, and the Levin–Tuchin law [40] for larger ones, $\boldsymbol{r} \gg 1/Q_s(x)$. Here, Q_s denotes the saturation momentum scale, which is the basic quantity characterizing the saturation effects, being related to a critical transverse size for the unitarization of the cross section, and is an increasing function of the energy [$Q_s^2 = Q_0^2 \, (\frac{x_0}{x})^{\lambda}$]. A fit to the structure function $F_2(x, Q^2)$ was performed in the kinematical range of interest, showing that it is not very sensitive to the details of the interpolation. The dipole-target forward scattering amplitude was parameterized as follows,

$$\mathcal{N}(x, \boldsymbol{r}) = \begin{cases} \mathcal{N}_0 \, \left(\frac{\boldsymbol{r} Q_s}{2} \right)^{2\left(\gamma_s + \frac{\ln(2/\boldsymbol{r}Q_s)}{\kappa \lambda Y}\right)} \ , & \text{for } \boldsymbol{r}Q_s(x) \leq 2 \, , \\ 1 - \exp^{-a \, \ln^2 (b \boldsymbol{r} Q_s)} , & \text{for } \boldsymbol{r}Q_s(x) > 2 \, , \end{cases} \tag{12}$$

where a and b are determined by continuity conditions at $\boldsymbol{r}Q_s(x) = 2$, $\gamma_s = 0.63$, $\kappa = 9.9$, $\lambda = 0.253$, $Q_0^2 = 1.0\,\text{GeV}^2$, $x_0 = 0.267 \times 10^{-4}$ and $\mathcal{N}_0 = 0.7$. Hereafter, we label the above model IIM. The first line from (12) describes the linear regime, whereas the second one describes saturation effects. When estimating the relative importance of saturation, we will switch off the second line of (12) and use only the first. This is a relevant check, since some observables may turn out to be completely insensitive to non-linear effects. Following [24], we generalize the IIM model for nuclear collisions assuming the following basic transformations: $\sigma_0 \to \sigma_0^A = A^{\frac{2}{3}} \times \sigma_0$ and $Q_s^2(x) \to Q_{s,A}^2 = A^{\frac{1}{3}} \times Q_s^2(x)$. As already emphasized in that reference, more sophisticated generalizations for the nuclear case are possible. However, as our goal is to obtain a first estimate of the saturation effects in these processes, our choice was to consider a simplified model that introduces a minimal set of assumptions. In a full calculation we must use the solution of the BK equation, obtained without disregarding the impact parameter dependence, as well as an initial condition constrained by current experimental data on the lepton-nucleus DIS.

3 Results

Before presenting our results for $\frac{\sigma_{\rm diff}}{\sigma_{\rm tot}}$ and for the diffractive structure function, let us investigate the mean dipole size dominating the diffractive cross section through the analysis of the photon-nucleus diffractive overlap function

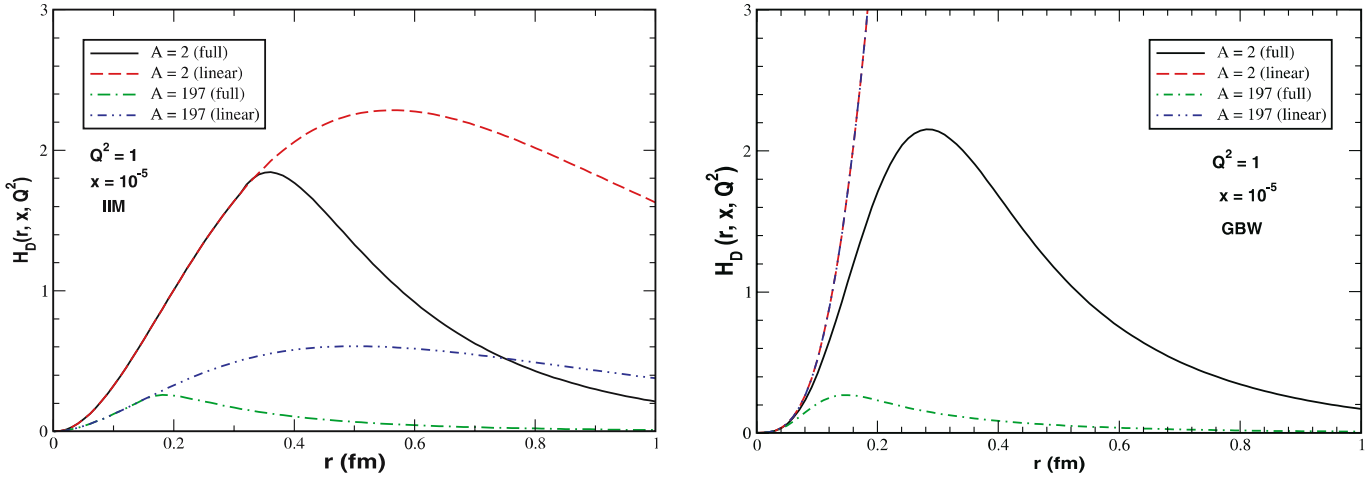

Fig. 1. The $\boldsymbol{r}$-dependence of the photon-nucleus diffractive overlap function (normalized by A^2) at different values of the atomic number and distinct saturation models: IIM (*left panel*) and GBW (*right panel*)

defined by

$$H_{\rm D}\,(\boldsymbol{r},x,Q^2) = 2\pi r \sum_{i=\rm T,L}\int d\alpha\,|\Psi_i(\alpha,\,\boldsymbol{r},Q^2)|^2\,\sigma^2_{\rm dip}(x,\boldsymbol{r},A)\,. \quad (13)$$

In Fig. 1, we present the $\boldsymbol{r}$-dependence of the photon-nucleus diffractive overlap function (normalized by A^2) at different values of the atomic number and $Q^2 = 1\,\mathrm{GeV}^2$. A similar analysis can be made for other values of Q^2. The main difference is that at large values of Q^2, the overlap function peaks at smaller values of the pair separation. For comparison, the predictions obtained with a generalization of the Golec-Biernat–Wüsthoff (GBW) model [6] for nuclear targets is also presented. When the saturation effects are included, the IIM and GBW overlap functions present a similar behavior, strongly reducing the contribution of large pair separations. At large A only small pair separations contribute to the diffractive cross section. However, in the linear case, these two models present a very distinct behavior, which is directly associated with the different prescription for the linear regime. While the GBW model assumes that $\sigma_{\rm dip} \propto \sigma_0 \boldsymbol{r}^2 Q_s^2$ in this regime, IIM assumes $\sigma_{\rm dip} \propto \sigma_0[\boldsymbol{r}^2 Q_s^2]^{\gamma_{\rm eff}}$, where $\gamma_{\rm eff} = \gamma_s + \ln(2/\boldsymbol{r}Q_s)/\kappa\,\lambda\,Y$ is smaller than one. Firstly, this implies a different A-dependence, since in the GBW model the product $[\sigma_0 Q_s^2]^2$ is proportional to A^2, which cancels with the normalization term. In the IIM model we have $[\sigma_0 Q_s^{2\gamma_{\rm eff}}]^2$, which implies an $A^{\frac{4+2\gamma_{\rm eff}}{3}}$-dependence. When combined with the factor A^2 that comes from the normalization, we expect an $A^{\frac{2(\gamma_{\rm eff}-1)}{3}}$-dependence for the IIM overlap function. As $\gamma_{\rm eff} < 1$, the overlap function decreases for large A also in the linear regime. This behavior is seen in Fig. 1. Secondly, in contrast to the GBW model, which predicts a $\boldsymbol{r}^2$ behavior for the dipole cross section in the linear regime, IIM leads to a $\boldsymbol{r}^{2\gamma_{\rm eff}}$ -dependence. This different prescription for the $\boldsymbol{r}$-dependence, when combined with the pair separation dependence of the wave functions, implies a strong modification of the contribution of large dipole sizes, as observed in Fig. 1. It is important to emphasize that this contribution dominates the cross section, i.e. if we disregard the saturation effects, the diffractive cross section is dominated by soft physics.

We now present a qualitative analysis of the A and energy dependence of the ratio $\sigma_{\rm diff}/\sigma_{\rm tot}$ using the IIM model

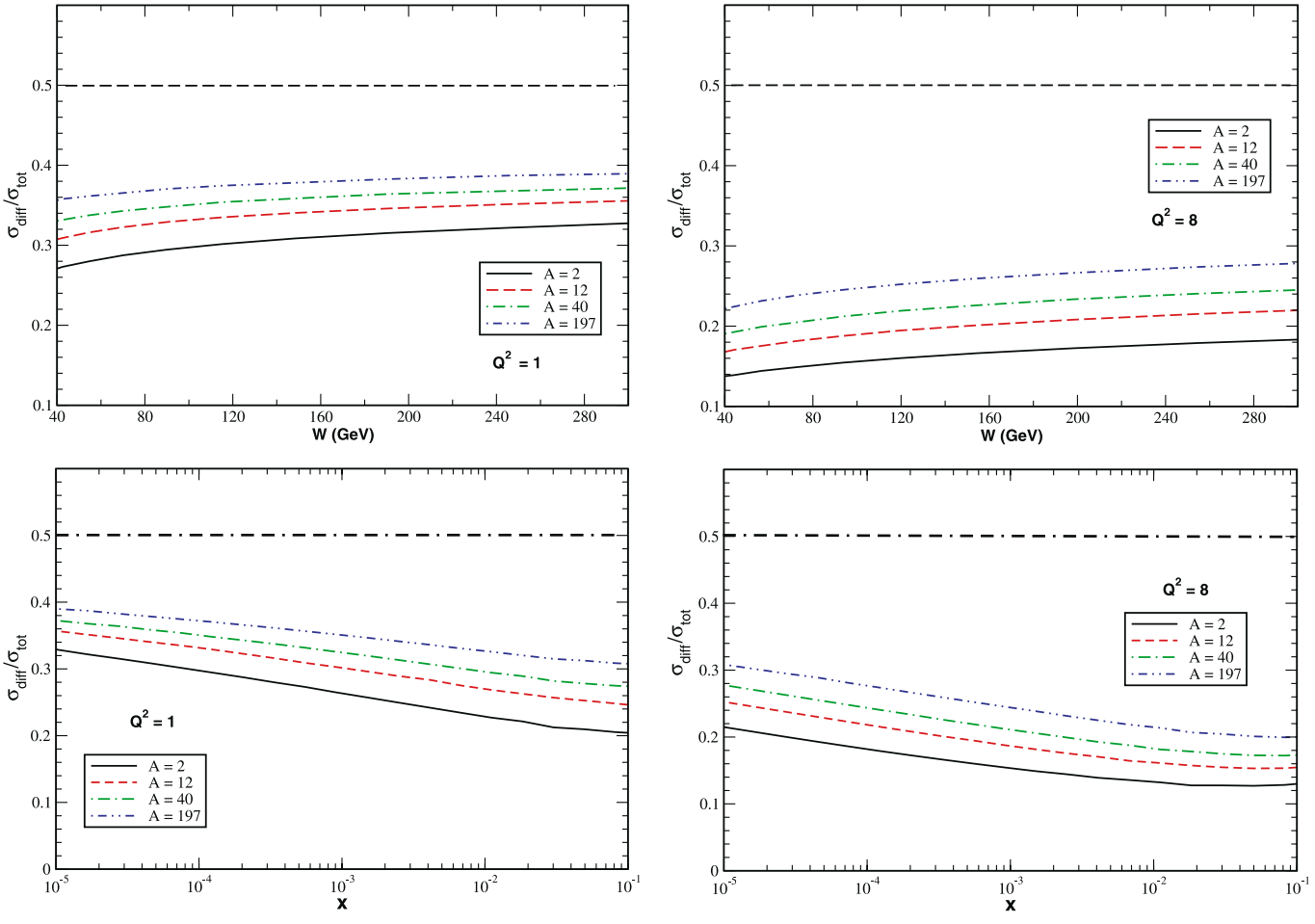

Fig. 2. The ratio between the diffractive and total cross sections as a function of x and W for different values of A and Q^2. The black disk limit, $\sigma_{\rm diff}/\sigma_{\rm tot} = 1/2$, is also presented

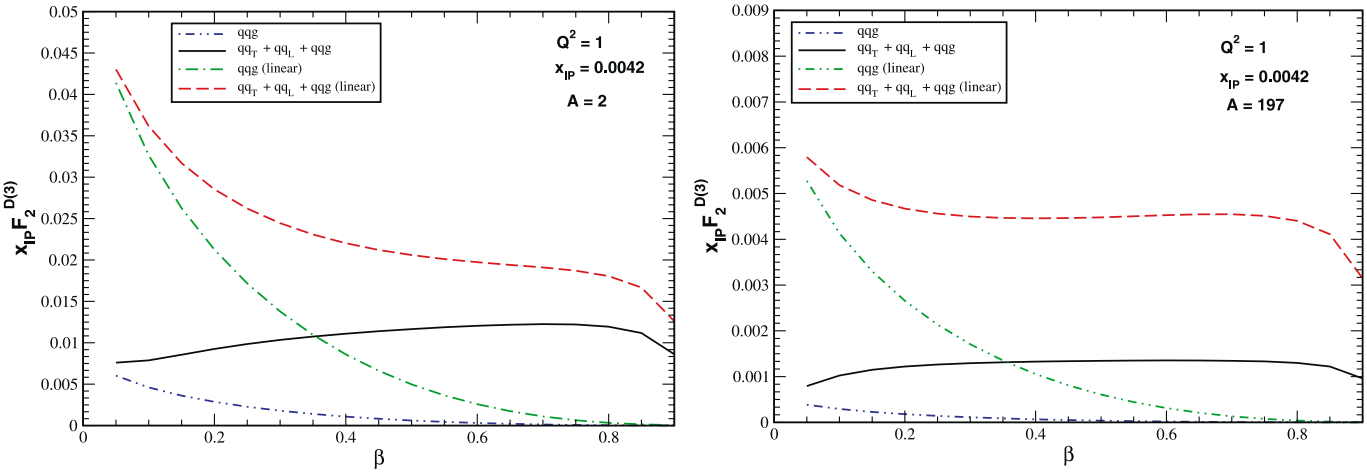

Fig. 3. Diffractive structure function $F_2^{\mathrm{D}(3)}$ as a function of β and distinct nuclei. The $q\bar{q}g$ component of the diffractive structure function is explicitly presented

generalized for nuclear targets. Following [6] and assuming that σ_{dip} in the saturation regime can be approximated by σ_0, the transverse part of the inclusive and diffractive cross sections, in the kinematical range where $Q^2 > Q_s^2$, can be expressed as

$$\sigma_{\mathrm{T}} \approx \int_0^{4/Q^2} \frac{\mathrm{d}\boldsymbol{r}^2}{\boldsymbol{r}^2}\sigma_0\Big[\frac{\boldsymbol{r}^2 Q_s^2}{4}\Big]^{\gamma_{\mathrm{eff}}} + \int_{\frac{4}{Q^2}}^{\frac{4}{Q_s^2}} \frac{\mathrm{d}\boldsymbol{r}^2}{\boldsymbol{r}^2}\left(\frac{1}{Q^2\boldsymbol{r}^2}\right)\sigma_0\Big[\frac{\boldsymbol{r}^2 Q_s^2}{4}\Big]^{\gamma_{\mathrm{eff}}} + \int_{4/Q_s^2}^{\infty} \frac{\mathrm{d}\boldsymbol{r}^2}{\boldsymbol{r}^2}\left(\frac{1}{Q^2\boldsymbol{r}^2}\right)\sigma_0 \qquad (14)$$

and

$$\sigma_{\mathrm{T}}^{\mathrm{D}} \approx \frac{1}{B_A}\left[\int_0^{4/Q^2} \frac{\mathrm{d}\boldsymbol{r}^2}{\boldsymbol{r}^2}\sigma_0^2\Big[\frac{\boldsymbol{r}^2 Q_s^2}{4}\Big]^{2\gamma_{\mathrm{eff}}} + \int_{\frac{4}{Q^2}}^{\frac{4}{Q_s^2}} \frac{\mathrm{d}\boldsymbol{r}^2}{\boldsymbol{r}^2}\left(\frac{1}{Q^2\boldsymbol{r}^2}\right)\sigma_0^2\Big[\frac{\boldsymbol{r}^2 Q_s^2}{4}\Big]^{2\gamma_{\mathrm{eff}}} + \int_{4/Q_s^2}^{\infty} \frac{\mathrm{d}\boldsymbol{r}^2}{\boldsymbol{r}^2}\left(\frac{1}{Q^2\boldsymbol{r}^2}\right)\sigma_0^2\right]. \qquad (15)$$

In order to obtain an approximated expression for the ratio, we will disregard the $\boldsymbol{r}$-dependence of the effective anomalous dimension, i.e. $\gamma_{\mathrm{eff}} = \gamma = \mathrm{cte}$. In this case, we obtain $\sigma_{\mathrm{diff}}/\sigma_{\mathrm{tot}} \approx [\frac{Q_s^2}{Q^2}]^{1-\gamma}$. Assuming $\gamma = 0.84$, as in [36], we predict that the ratio decreases with the photon virtuality and presents a weak energy dependence. However, analyzing the A-dependence, we expect a growth of approximately 30% when we increase A from 2 to 197. In the kinematical range, where $Q^2 < Q_s^2$, the ratio of cross sections presents a similar behavior. The main difference is that in the asymptotic regime of very large energies, the cross section for diffraction reaches the black disk limit of 50% of the total cross section.

In Fig. 2, we show the ratio $\sigma_{\mathrm{diff}}/\sigma_{\mathrm{tot}}$, computed with the help of (3) and (4), as a function of W and x for different values of A. The black disk limit, $\sigma_{\mathrm{diff}}/\sigma_{\mathrm{tot}} = 1/2$, is also presented in the figure. We can see that the ratio depends weakly on W and on x but is strongly suppressed for increasing Q^2. This suggests that in the deep perturbative region, diffraction is more suppressed. This same behavior was observed in diffractive ep data [26]. Moreover, the energy dependence of the ratio is remarkably flat, increasing with A, becoming 37% (30%) larger for gold in comparison to proton (deuteron). This behavior agrees qualitatively with the previous calculation of [32] and with our previous estimate. Similar results have been obtained in the pioneering work of [28] in a different context. The appearance of a large rapidity gap in 37% of all eA scattering events would be a striking confirmation of the saturation picture.

In Fig. 3, we show our predictions for the diffractive structure functions $x_{I\!P}F_2^{\mathrm{D}(3)}(x_{I\!P}, \beta, Q^2)$ as functions of β and different nuclei. We also present the linear prediction for $x_{I\!P}F_2^{\mathrm{D}(3)}$. It is important to emphasize that a linear ansatz for the dipole cross section would not describe the HERA data. However, in order to estimate the importance of the saturation physics and clarify its contribution at different kinematical ranges, a comparison between these two predictions is valid. We can see that the normalization of $x_{I\!P}F_2^{\mathrm{D}(3)}$ is strongly reduced increasing the atomic number, which is expected from our analysis of the diffractive overlap function. Moreover, although the photon wave function determines the general structure of the β-spectrum [6, 37], the $q\bar{q}g$ component, which dominates the region of small β, has its behavior modified by saturation effects and changes the behavior of $x_{I\!P}F_2^{\mathrm{D}(3)}$ in this region. Moreover, the diffractive structure function becomes almost flat at intermediate values of β and large A. In Fig. 4, we show an amplification of the lower curves in Fig. 3 and also include the $q\bar{q}_{\mathrm{T}}$ component. In doing this, another interesting feature of diffraction off nuclear targets emerges, namely, the relative reduction of the $q\bar{q}g$ component with respect to $q\bar{q}$.

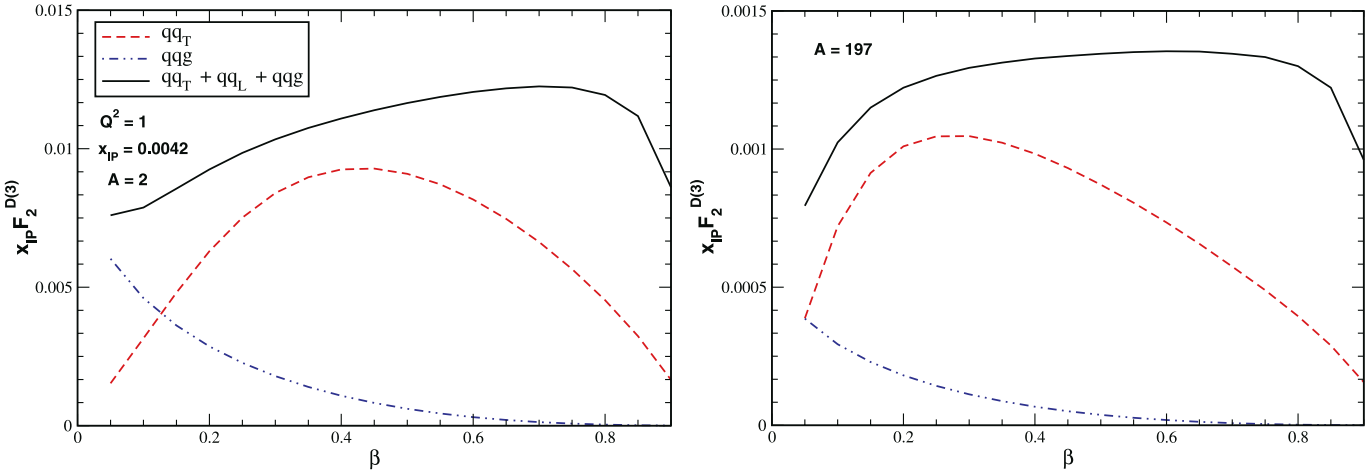

Fig. 4. Diffractive structure function $F_2^{\mathrm{D}(3)}$ as a function of β and distinct nuclei. The transverse and $q\bar{q}g$ components of the diffractive structure function are explicitly presented

In Fig. 5, we show our predictions for $x_{I\!P} F_2^{\mathrm{D}(3)}(x_{I\!P}, \beta, Q^2)$ as a function of $x_{I\!P}$ and different values of β, Q^2 and A. Our choice for the combination of values of β and Q^2 was motivated by the HERA results [26]. The $x_{I\!P}$-dependence comes from the dipole cross section, which in our case is given by the IIM model generalized to nuclear targets. We find that $x_{I\!P} F_2^{\mathrm{D}(3)}$ increases at small values of $x_{I\!P}$. However, as the saturation scale grows with A, the $x_{I\!P}$ becomes weaker when we increase the atomic number.

In Fig. 6 we show our predictions for the ratio

$$R^{\mathrm{diff}}_{A1,A2}(\beta, Q^2, x_{I\!P}) = \frac{F^{\mathrm{D}(3)}_{2,A1}(\beta, Q^2, x_{I\!P})}{F^{\mathrm{D}(3)}_{2,A2}(\beta, Q^2, x_{I\!P})}$$

as a function of β and $x_{I\!P}$. In our calculation we assume that $A_2 = 2$. Our analysis is motivated by [25, 27]. In these papers it was suggested that the nuclear dependence of this ratio can help us to establish the universality of the pomeron structure. In particular, in [27], the authors have pointed out that if $R^{\mathrm{diff}}_{A1,A2}(\beta, Q^2, x_{I\!P}) = 1$ one can conclude that the structure of the pomeron is universal and the pomeron flux is A-independent. On the other hand, if $R^{\mathrm{diff}}_{A1,A2}(\beta, Q^2, x_{I\!P}) = f(A_1, A_2)$, the structure is universal but the flux is A-dependent. From our previous analysis we can anticipate that in the dipole picture, assuming the presence of saturation effects, this ratio will be A-dependent. Moreover, its behavior will be determined by the saturation scale. In Fig. 6, we observe a strong decrease of $R^{\mathrm{diff}}_{A1,A2}$ as a function of A. At the same time, this ratio

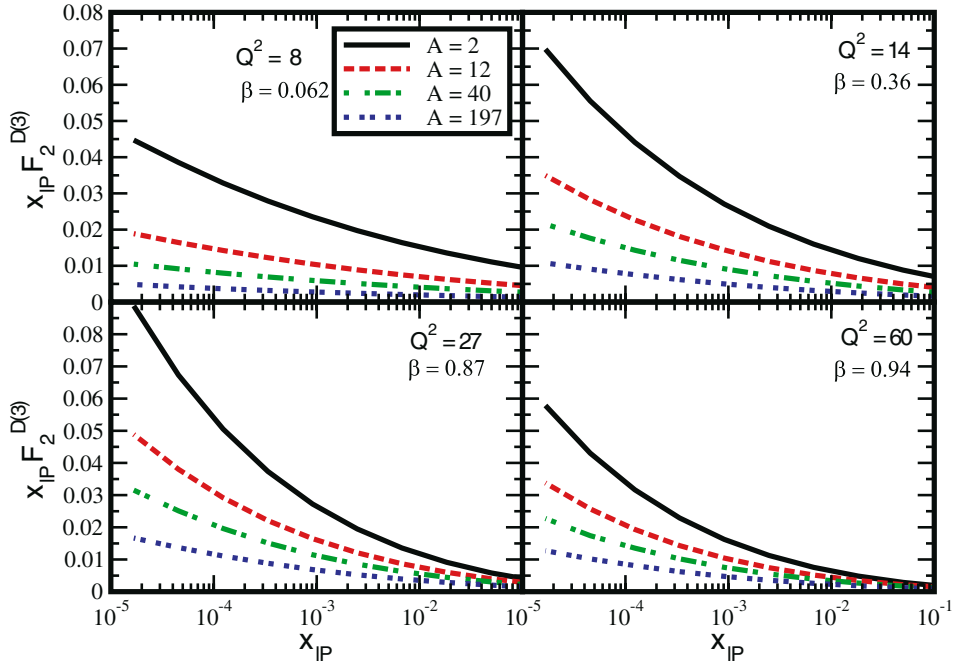

Fig. 5. Predictions for the diffractive structure functions $x_{I\!P} F_2^{\mathrm{D}(3)}(x_{I\!P}, \beta, Q^2)$ plotted as a function of $x_{I\!P}$ for different values of β, Q^2 and A

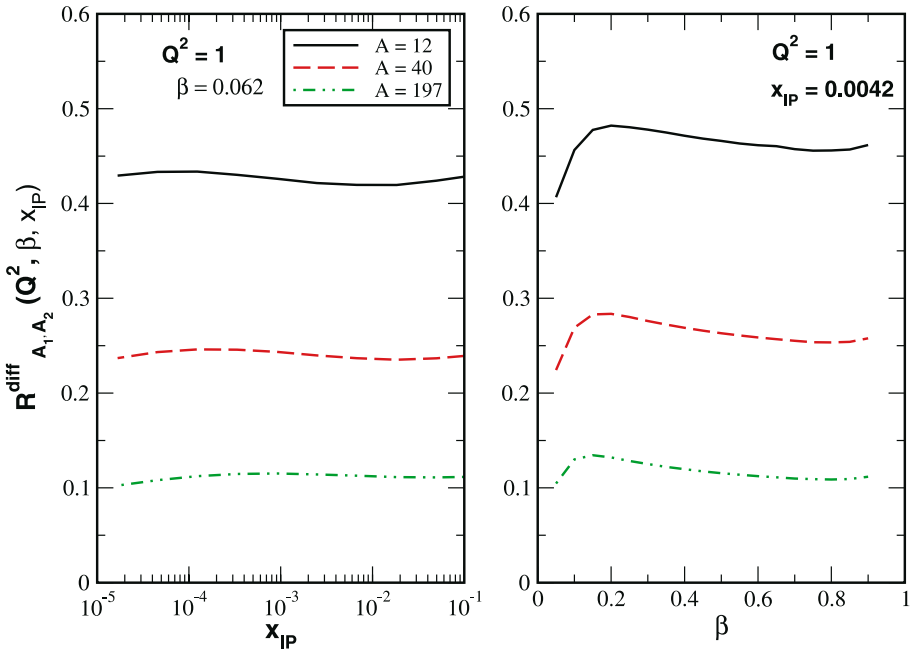

Fig. 6. The ratio $R^{\rm diff}_{A1,A2}(Q^2,\beta, x_{I\!P}) = \frac{F^{D(3)}_{2,A1}(Q^2,\beta,x_{I\!P})}{F^{D(3)}_{2,A2}(Q^2,\beta,x_{I\!P})}$ as a function of $x_{I\!P}$ and β. Comparison between the predictions for the ratio at different values of A_1

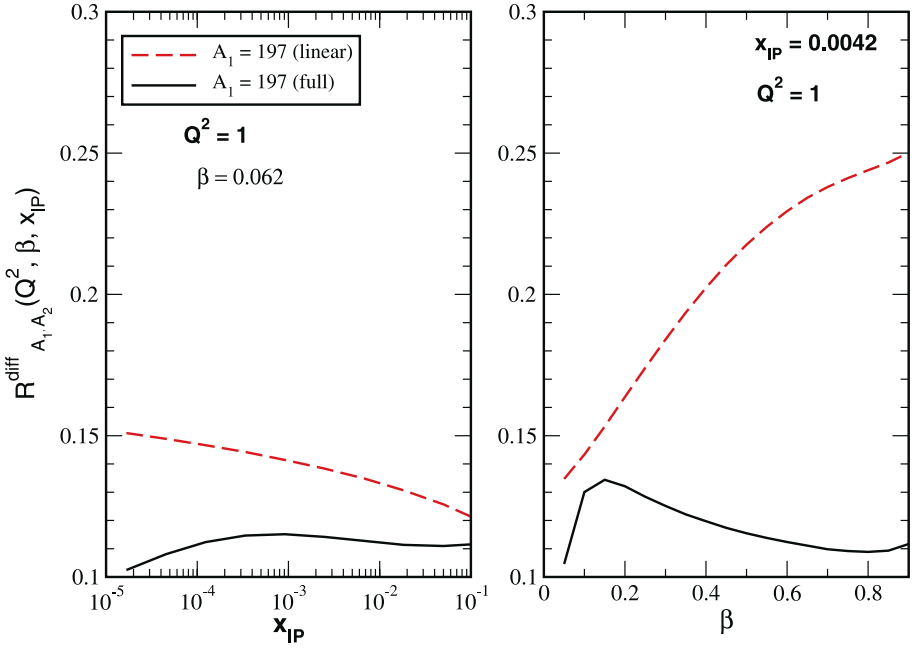

Fig. 7. The ratio $R^{\rm diff}_{A1,A2}(Q^2,\beta, x_{I\!P}) = \frac{F^{D(3)}_{2,A1}(Q^2,\beta,x_{I\!P})}{F^{D(3)}_{2,A2}(Q^2,\beta,x_{I\!P})}$ as a function of $x_{I\!P}$ and β. Comparison between the saturation and linear predictions

is remarkably flat at all values of A, $x_{I\!P}$ and $\beta \geq 0.2$. However, at small β, it presents a steeper dependence directly associated with the nuclear dependence of the $q\overline{q}g$ component of the diffractive structure function (see Fig. 4). In order to estimate how much of the flat behavior is due to saturation, we calculate $R^{\rm diff}_{A1,A2}$ again using only the linear part of the dipole cross section, as discussed above, for the heaviest target ($A = 197$), for which the saturation effects are expected to be dominant and show our results in Fig. 7. As can be seen, saturation is largely responsible for the weak dependence of $R^{\rm diff}_{A1,A2}$ on $x_{I\!P}$ and β. In [27] the possibility that the A -dependence of $R^{\rm diff}_{A1,A2}$ can be described by the ratio between the inclusive nuclear structure functions was suggested for the case of an A-dependent pomeron structure and an A-independent flux. We have checked this conjecture using the results from [24] and have found that it fails, the inclusive ratio being larger than the diffractive one.

4 Summary

Diffractive physics in nuclear DIS experiments has been studied at the electron-ion collider eRHIC. Hence it is in-

teresting to extend the current ep predictions to the corresponding energy and targets that will be available in this collider. In this work, we address nuclear diffractive DIS and compute observable quantities like $\sigma_{\rm diff}/\sigma_{\rm tot}$ and $F_2^{\rm D(3)}$ in the dipole picture. In particular, we have investigated the potential of eA collisions as a tool for revealing the details of the saturation regime. Since $\sigma_{\rm diff}$ is proportional to $\sigma^2_{\rm dip}$, diffractive processes are expected to be particularly sensitive to saturation effects. Moreover, due to the highly non-trivial A-dependence of $\sigma_{\rm dip}$, diffraction off nuclear targets is even more sensitive to non-linear effects. Using well-established definitions of $\sigma_{\rm diff}$ and $F_2^{\rm D(3)}$ and a recent and successful parameterization of $\sigma_{\rm dip}$, we have studied observables that may serve as signatures of the color glass condensate. Without adjusting any parameter, we have found that the ratio $\sigma_{\rm diff}/\sigma_{\rm tot}$ is a very flat function of the center-of-mass energy W, in good agreement with existing HERA data. Extending the calculation to nuclear targets, we have shown that this ratio remains flat and increases with the atomic number. At larger nuclei we predict that approximately 37% of the events observed at eRHIC are diffractive. Moreover, we have analyzed the behavior of the diffractive structure function $F_2^{\rm D(3)}$ and found that in certain regions of the β - $x_{I\!P}$ space, the diffractive structure function $F_2^{\rm D(3)}$ decreases up to an order of magnitude when going from the lightest to the heaviest targets. Finally, we have found that, for nuclear targets, the contribution of the $q\overline{q}g$ Fock state becomes less important.

Considering the results obtained in this paper and those presented in [24], we can conclude that eA collisions are very promising for the experimental confirmation of the non-linear effects of QCD.

Acknowledgements. V.P. Gonçalves thanks Magno Machado for informative and helpful discussions. This work was partially financed by the Brazilian funding agencies CNPq, FAPESP and FAPERGS.

References

1. E. Iancu, R. Venugopalan, arXiv:hep-ph/0303204
2. A.M. Stasto, Acta Phys. Polon. B **35**, 3069 (2004)
3. H. Weigert, Prog. Part. Nucl. Phys. **55**, 461 (2005)
4. J. Jalilian-Marian, Y.V. Kovchegov, Prog. Part. Nucl. Phys. **56**, 104 (2006)
5. J.P. Blaizot, F. Gelis, Nucl. Phys. A **750**, 148 (2005)
6. K. Golec-Biernat, M. Wüsthoff, Phys. Rev. D **59**, 014017 (1999); ibid. **D60**, 114023 (1999)
7. M. Wusthoff, A.D. Martin, J. Phys. G **25**, R309 (1999)
8. A. Hebecker, Phys. Rept. **331**, 1 (2000)
9. V. Barone, E. Predazzi, *High-Energy Particle Diffraction*, (Springer, Berlin Heidelberg New York, 2002)
10. J.R. Forshaw, R. Sandapen, G. Shaw, Phys. Lett. B **594**, 283 (2004)
11. A.D. Martin, M.G. Ryskin, G. Watt, Eur. Phys. J. C **44**, 69 (2005)
12. S.J. Brodsky, R. Enberg, P. Hoyer, G. Ingelman, Phys. Rev. D **71**, 074020 (2005)
13. N.N. Nikolaev, B.G. Zakharov, Z. Phys. C **49** 607 (1991); Z. Phys. C **53**, 331 (1992)
14. A.H. Mueller, Nucl. Phys. B **415**, 373 (1994); A.H. Mueller, B. Patel, Nucl. Phys. B **425**, 471 (1994)
15. I.I. Balitsky, Nucl. Phys. B **463**, 99 (1996); Y.V. Kovchegov, Phys. Rev. D **60**, 034008 (1999)
16. Y.V. Kovchegov, E. Levin, Nucl. Phys. B **577**, 221 (2000)
17. A. Kovner, U.A. Wiedemann, Phys. Rev. D **64**, 114002 (2001)
18. M. Hentschinski, H. Weigert, A. Schafer, arXiv:hep-ph/0509272
19. M.B. Gay Ducati, V.P. Goncalves, M.V.T. Machado, Phys. Lett. B **506**, 52 (2001)
20. M.B. Gay Ducati, V.P. Goncalves, M.V.T. Machado, Nucl. Phys. A **697**, 767 (2002)
21. S. Munier, A. Shoshi, Phys. Rev. D **69**, 074022 (2004)
22. K. Golec-Biernat, C. Marquet, Phys. Rev. D **71**, 114005 (2005)
23. V.P. Goncalves, M.V.T. Machado, Phys. Lett. B **588**, 180 (2004)
24. M.S. Kugeratski, V.P. Goncalves, F.S. Navarra, arXiv:hep-ph/0508255
25. A. Despande, R. Milner, R. Venugopalan, W. Vogelsang, Ann. Rev. Nucl. Part. Sci. **55**, 165 (2005)
26. [ZEUS Collaboration], J. Breitweg et al. , Eur. Phys. J. **C6**, 43 (1999); [ZEUS Collaboration], S. Chekanov et al., Eur. Phys. J. **C38**, 43 (2004); C. Adloff et al. [H1 Collaboration], Z. Phys. C **76**, 613 (1997)
27. Arneodo M, et al., In: Proceedings of "Future Physics at HERA", DESY, September 1995, arXiv:hep-ph/9610423
28. N.N. Nikolaev, B.G. Zakharov, V.R. Zoller, Z. Phys. A **351**, 435 (1995)
29. Y.V. Kovchegov, L.D. McLerran, Phys. Rev. D **60**, 054025 (1999); [Erratum-ibid. D **62**, 019901 (2000)]
30. E. Gotsman, E. Levin, M. Lublinsky, U. Maor, K. Tuchin, Phys. Lett. B **492**, 47 (2000)
31. E. Gotsman, E. Levin, U. Maor, L.D. McLerran, K. Tuchin, Nucl. Phys. A **683**, 383 (2001)
32. E. Levin, M. Lublinsky, Nucl. Phys. A **712**, 95 (2002)
33. V.P. Goncalves, M.V.T. Machado, Eur. Phys. J. C **30**, 387 (2003)
34. V.P. Goncalves, M.V.T. Machado, Eur. Phys. J. C **38**, 319 (2004)
35. L. Frankfurt, V. Guzey, M. Strikman, Phys. Lett. B **586**, 41 (2004)
36. E. Iancu, K. Itakura, S. Munier, Phys. Lett. B **590**, 199 (2004)
37. M. Wusthoff, Phys. Rev. D **56**, 4311 (1997)
38. N.N. Nikolaev, B.G. Zakharov, J. Exp. Theor. Phys. **78**, 598 (1994) [Zh. Eksp. Teor. Fiz. **105**, 1117 (1994)]; Z. Phys. C **64**, 631 (1994); N.N. Nikolaev, W. Schaefer, B.G. Zakharov, V.R. Zoller, JETP Lett. **80**, 371 (2004) [Pisma Zh. Eksp. Teor. Fiz. **80**, 423 (2004)]
39. H. Abramowicz, L. Frankfurt, M. Strikman, Surveys High Energ. Phys. **11**, 51 (1997)
40. E. Levin, K. Tuchin, Nucl. Phys. B **573**, 833 (2000)